Low-Temperature Ignition and Oxidation Mechanisms of Tetrahydropyran

Samuel W. Hartness^a, Marwa Saab^b, Matthias Preuβker^c, Rosalba Mazzotta^a Nicholas S. Dewey^d, Annabelle W. Hill^d, Guillaume Vanhove^b, Yann Fenard^b, K. Alexander Heufer^c, Brandon Rotavera^{a,d,*}

^aCollege of Engineering, University of Georgia, Athens, GA 30602

^bPhysical Chemistry of Combustion Processes and the Atmosphere, University of Lille, Lille, France

^cHigh-Pressure Gas Dynamics, Shock Wave Laboratory, RWTH Aachen University, Aachen, Germany

^dDepartment of Chemistry, University of Georgia, Athens, GA 30602

Abstract

Cyclic ethers are relevant as next-generation biofuels and are also combustion intermediates that directly follow from unimolecular decomposition of hydroperoxyalkyl radicals. Accordingly, cyclic ether reactions are crucial to understanding low-temperature oxidation for advanced compression-ignition combustion applications where peroxy radials are central to degenerate chain-branching pathways. Reaction mechanisms relevant to low-temperature ignition of cyclic ethers contain intrinsic complexities due to competing reactions of carbon-centered radicals formed in the initiation step undergoing either reactions with O_2 or ring-opening. To gain insight into mechanisms describing tetrahydropyran combustion, ignition delay time and speciation measurements were conducted. The present work integrates measurements below 1000 K of ignition delay times and species profiles in rapid compression machine experiments from 5 bar -20 bar, spanning several equivalence ratios, with jet-stirred reactor experiments at 1 bar and stoichiometric conditions to provide the first set of data on tetrahydropyran combustion at temperatures where peroxy radical reactions dominate. The experiments are complemented with the development of the first chemical kinetics mechanism for tetrahydropyran that includes peroxy radical reactions, including O_2 -addition to tetrahydropyranyl ($\dot{Q}OOH$), cyclic ether formation, β -scission of $\dot{Q}OOH$, and ketohydroperoxide formation.

Negative-temperature coefficient (NTC) behavior is exhibited in the experiments and is reflected in the model predictions, which were within experimental uncertainty for several conditions. Disparities between the model predictions and experiments were analyzed via sensitivity analysis to identify contributing factors from elementary reactions. The analyses examine the role of ring-opening products of tetrahydropyranyl and hydroperoxytetrahydropyranyl isomers to identify reaction mechanisms that may contribute to model uncertainties. The detection of 66 species in the JSR experiments indicates that tetrahydropyran undergoes complex reaction networks, which include alkyl radical reactions and aldehyde radical reactions. Primary radicals pentanal-5-yl and butanal-4-yl are derived from ring-opening reactions of tetrahydropyran-1-yl and undergo subsequent decarbonylation to form alkyl radicals that undergo reaction with O₂ and may contribute to chain-branching, in addition to pathways involving tetrahydropyran-derived ketohydroperoxides.

Keywords: cyclic ether, rapid compression machine, peroxy radicals, autoignition, jet-stirred reactor

^{*}Corresponding author.

Information for Colloquium Chairs and Cochairs, Editors, and Reviewers

1) Novelty and Significance Statement

Novelty:

- We provide the first detailed chemical kinetics model for tetrahydropyran a cyclic ether biofuel and an intermediate of *n*-alkane oxidation that includes peroxy-radical chemistry to enable better understanding of low-temperature combustion behavior.
- Our paper provides the first ignition delay time measurements for tetrahydropyran below 1000 K.
- We also provide the first speciation measurements from low-temperature oxidation of tetrahydropyran.
- We expand the state of knowledge on cyclic ether chemistry including ring-opening reactions by uncovering connections to aldehydes and competing reactions channels with O₂.

Significance: This paper brings to light several fundamental kinetics aspects of cyclic ether oxidation, including the role of ring-opening kinetics of R and QOOH radicals, and related impact on ignition chemistry. Our findings are significant as they expand the understanding of the low-temperature chemical kinetics of a novel biofuel. Moreover, the experiments and modeling highlight clear connections of tetrahydropyran combustion to oxidation of radicals common to other fuels including *n*-butane, diethyl ether, and tetrahydrofuran. This is significant because it underscores the value of sub-mechanisms of several classes of species to the development of a detailed mechanism. Lastly, we identify important shortcomings that must be investigated in a future study to improve model accuracy for simulating tetrahydropyran oxidation and similar biofuels for the benefit of increasing the sustainability of the combustion-derived energy for the transportation sector.

2) Author Contributions

- SH: Writing/Draft, Methodology, Measurements, Modeling, Formal Analysis
- MS: Measurements, Modeling, Formal Analysis
- MP: Measurements, Formal Analysis
- RM: Measurements, Formal Analysis
- ND: Measurements
- AH: Measurements
- GV: Methodology, Writing/Editing
- YF: Kinetic Model Development, Writing/Editing
- KAH: Methodology, Formal Analysis, Writing/Editing
- BR: Conceptualization, Formal Analysis, Writing/Editing

3) Authors' Preference and Justification for Mode of Presentation at the Symposium

The authors prefer the oral presentation paper (**OPP**) option at the Symposium, for the following reasons:

- 1. We highlight fundamental kinetics questions that will spur research activities of experimentalists and theoreticians.
- Presentation of this work will motivate the community for discussions on new experimental and modeling efforts on dicarbonyls, relevant to cyclic ethers and ketohydroperoxide chemistry.
- 3. Our paper produces new insight that impacts kinetics modeling approaches toward cyclic ethers.
- 4. We contribute to three of the four themes of the 40th Symposium: *Combustion Fundamentals*, *Combustion Research Tools*, and *Combustion Impact and Mitigation*. Our paper is not part of a broader set of work requiring extensive background for an engaging presentation.

1 1. Introduction

Utilization of next-generation biofuels remains of interest for reducing the carbon intensity of the 4 transportation sector. Continuing advances in 5 catalysis create improved synthesis routes for 6 lignocellulosic biofuels, such as tetrahydropyran [1, 7 2]. Incorporating tetrahydropyran in advanced 8 compression-ignition technologies requires 9 understanding of reaction pathways that describe low-10 temperature oxidation, which is driven by reactions of 11 carbon-centered radicals (R) with O₂ that form peroxy 12 radicals (ROO) and subsequent hydroperoxy-13 substituted radicals, QOOH (Fig. 1). Moreover, 14 because cyclic ether oxidation is complex due to ring-15 opening reactions [3, 4], detailed understanding relies 16 on both experimental and modeling approaches.

Figure 1: Molecular structures of tetrahydropyran with distinct H-abstraction sites, and example ROO and QOOH with notation for peroxy group and localized radical sites.

Several studies on high-temperature combustion of 18 tetrahydropyran are reported. Dagaut et al. [5] 19 measured ignition delay times and species profiles 20 from 800 - 1700 K and generated the first chemical 21 kinetics mechanism. Labbe et al. [6] conducted 22 laminar flame experiments and generated a detailed 23 mechanism drawing analogy to cyclohexane. Tran et 24 al. [7] developed a mechanism to compare to 25 pyrolysis experiments, premixed flame experiments, 26 and shock tube experiments. Despite progress on 27 chemical kinetics mechanisms, however, none 28 include peroxy-radical reactions necessary for 29 describing low-temperature oxidation.

Low-temperature combustion studies 31 tetrahydropyran are also reported. Rotavera et al. [8] 32 examined the effect of the ether group on chainreactions multiplexed-33 terminating using mass-spectrometry (MPIMS) 34 photoionization experiments and theoretical rate calculations. Yields 36 of conjugate alkenes from chain-terminating pathways produced via \dot{R} + O_2 reactions were 38 favorable up to ~600 K, yet diminished with 39 increasing temperature due to ring-opening of initial 40 R radicals. Chen et al. [9] measured time-dependent 41 yields of OH and HOO between 500 - 750 K in 42 tetrahydropyran and cyclohexane oxidation using 43 multi-pass near-IR absorption spectroscopy. In 44 addition, the presence of the cyclic ether group 45 created additional pathways to form OH and HOO 46 from ring-opening of R and QOOH radicals. Davis et 47 al. [10] studied the reaction mechanisms of 48 tetrahydropyran and cyclohexane oxidation from 500 49 - 700 K via MPIMS experiments and theoretical 50 calculations to examine the effect of the cyclic ether

51 on ketohydroperoxide formation. The cyclic ether 52 group rendered ring-opening reactions more facile, 53 leading to lower ketohydroperoxide yields direct from 54 tetrahydropyran compared to cyclohexane, due to 55 unimolecular decomposition of QOOH that precludes 56 second-O₂-addition.

The present work provides extensive experimental 58 measurements from multiple apparatus and the 59 development of the first chemical kinetics mechanism 60 for modeling low-temperature combustion of 61 tetrahydropyran. Ignition times are reported for 62 tetrahydropyran at low-temperatures for the first time 63 and are measured in rapid compression machine 64 (RCM) experiments along with time-dependent 65 species profiles. Species profiles are measured in a 66 jet-stirred reactor (JSR) for the first time in the low-67 temperature regime from 500 – 900 K. Simulations of 68 ignition delay times and species profiles with the new model highlight the impact of the cyclic ether functional group on low-temperature combustion systems through its introduction of favorable ringopening reactions and, critically, consequent aldehyde 73 chemistry that links the oxidation of tetrahydropyran 74 to the oxidation of 1-propyl and 1-butyl.

76 2. Experimental and Modeling Approach

The following sections concisely describe the RCM measurements at the RWTH Aachen facility (*Section 9 2.1*), RCM measurements at the University of Lille 80 facility (*Section 2.2*), JSR measurements at the University of Georgia (*Section 2.3*), and the approach 82 for the development of the chemical kinetics 83 mechanism (*Section 2.4*).

85 2.1 RCM measurements (Aachen)

Ignition delay times were measured in a single, 87 creviced-piston RCM detailed in Ramalingam et al. 88 [11]. An adjustable endwall allows for variation of the 89 compression ratio and therefore alteration of the end-90 of-compression (EOC) temperature without altering 91 the bath gas composition (mole fractions in Table 92 S1a). The creviced-piston ensures an adiabatic core 93 by suppressing roll-up vortices. Non-reactive pressure 94 traces (located in S1b) are measured with a Kistler 95 pressure sensor (6125C-U20) and collected at each 96 condition by replacing O₂ with N₂. The non-reactive 97 trace allows for a volume profile to be derived to 98 account for facility effects [12]. Overall uncertainties in the EOC conditions are approximately ± 5 K in end 100 of compression temperature (T_C) and $\pm 0.5\%$ in end of 101 compression pressure (Pc) [13]. The ignition delay 102 times, defined as the time between EOC and the 103 highest rate of pressure increase afterwards, were 104 measured for tetrahydropyran at 10 bar and 20 bar using equivalence ratios (ϕ) of 0.5, 1.0, and 2.0, where 106 ϕ is defined as the ratio of tetrahydropyran: O₂ for the 107 actual condition relative to the stoichiometric 108 condition. Tc covered ~600 – 1000 K.

111

110

84

112 2.2 RCM measurements (Lille)

Ignition delay times were also measured in a single, creviced-piston RCM with a right-angle design detailed in Mergulhão et al. [14]. The right-angle 115 design maintains the combustion chamber volume constant after EOC and T_C is controlled through changing the bath gas composition (mole fractions in Table S1c). From Bourgeois et al. [15], a 45-ms compression time is used in conjunction with the creviced-piston to minimize piston roll-up vortex 121 formation. Pressure traces are measured using a Kistler pressure transducer (6052) and charge amplifier (5018). Uncertainties in T_C and P_C are $\pm 5~K$ 125 and ± 0.1 bar respectively. Non-reactive pressure traces are measured through substitution of N₂ for O₂ in the bath gas (located in **S1d**). Ignition delay times were measured at stoichiometric conditions for P_C of 5, 10, and 15 bar. 129

Time-dependent species profiles are measured by 130 sampling the reactive mixture at different times 131 between the EOC and total ignition, in a series of RCM experiments at the same condition. Sampled gases were quenched via expansion cooling into a 134 heated chamber ~40 times the volume of the 135 combustion chamber. Gas-sampling was conducted when EOC conditions were 730 K and 10 bar using a diluted stoichiometric mixture (mole fractions of 1.41%, 9.86%, and 88.77% for tetrahydropyran, O₂, 139 and N₂ respectively) that led to an extended ignition delay (53.4 ms) against which time is normalized for the reported species concentrations. Following gas 143 chromatographic separation, O2 and CO are 144 quantified using a thermal conductivity detector 145 (TCD) while all other species are analyzed with a 146 flame ionization detector (FID). The results were 147 corrected from crevice volume dilution as described 148 in [14]. The uncertainty of the measured species mole 149 fractions is $\pm 10\%$ for calibrated species with TCD and 150 FID, and $\pm 20\%$ for species quantified using the effective carbon number with FID [16]. 151

153 2.3 JSR measurements – (Georgia)

152

Species profiles were measured using a 33.5 cm³ 154 jet-stirred reactor following the design in Dagaut et al. 156 [17] described in Hartness et al. [18] and Koritzke et 157 al. [19]. Thermal-based mass flow controllers deliver O₂ and N₂ to the reactor. Gas-phase tetrahydropyran is delivered with N2 through a separate capillary by a temperature-programmed vapor delivery system maintained at 60 ± 1 °C, which uses a Coriolis liquid flow controller. Experiments were conducted at a 163 residence time of 4.0 ± 0.1 s and covered 500 - 900 K 164 in 25 K increments at stoichiometric conditions. 165 Reactor pressure was maintained at 835 ±4 Torr via 166 PID control. The concentrations of tetrahydropyran and oxygen were maintained at 0.5% and 3.5% by volume with N2 as the balance. 168

169 Temperature gradients, measured across the 170 \sim 3.2cm reactor centerline with a K-type 171 thermocouple, are at most $\pm 0.8\%$ of the nominal 172 temperature due to PID control of four heating plates.

173 Sampling occurs through a quartz sonic probe, 174 positioned at 1.5 cm from the center of the reactor that 175 quenches the sample and sends cooled extracted gases 176 into a quartz cell via inert-coated lines maintained at 177 70 °C. The quartz cell is connected to an inert-coated 178 compression cell maintained at 70 °C which supplies 179 the gases to a GC.

180 $m H_2$, O₂, CO, CH₄, and CO₂ are quantified via 181 packed column separation and a TCD. The remaining 182 gas is split into two equal volumes and injected onto 183 separate, identical columns that follow the same 184 temperature programming, one leading to a 70-eV 185 electron-impact ionization mass spectrometer (EI-186 MS) and the other to a vacuum-ultraviolet absorption 187 cell (VUV) maintained at 110 ± 1 °C and 800 ± 8 Torr.

Reference measurements are conducted on 189 calibration mixtures produced manometrically, 190 typically at 500 ppm, and injected onto the GC 191 columns leading to the EI-MS and VUV detectors 192 along with a 1% N₂O internal standard. MS and VUV 193 spectra for all species are in S2. The use of the two 194 detectors in tandem with GC allows for cross-195 validation of species quantification, at concentrations 196 as low as 1 ppm, via several methods explained in S3 197 and for identification of stereoisomers 198 constitutional isomers. Uncertainties 199 concentrations were calculated by species from repeat 200 experiments and are <10% except in the case of 201 pentanedial (S3). The method used to measure a 202 reference spectrum for pentanedial relied on injection 203 of an aqueous pentanedial solution into the GC. The 204 variance between the reference spectra was \sim 7%. The 205 calculated experimental uncertainty is $\pm 20\%$ on 206 average when comparing repeat experiments, likely 207 due to the low vapor pressure (~15 mTorr at 20 °C).

209 2.4 chemical kinetics mechanism development

Unimolecular reactions, H-abstraction, and β -211 scission reactions and corresponding rate parameters 212 from Tran et al. [7] were utilized along with some 213 modifications (vide infra) and integrated into a base 214 mechanism, NUIGmech1.1 [20]. H-abstraction 215 reactions by OH from Tran et al. [7], which were 216 developed using the correlation of Dean and Bozzelli 217 [21], were adopted. H-abstraction reactions by HOO 218 are of moderate sensitivity in high-temperature 219 experiments, as in Tran et al. [7], yet are of elevated 220 importance at low-to-intermediate temperatures for 221 tetrahydropyran oxidation, where HOO production 222 and H-abstraction are more facile due to the cyclic 223 ether group [8, 9]. The rate coefficient measured for 224 HOO + cyclohexane [22] was adopted. The activation 225 energy is decreased by 1.5 kcal-mol⁻¹ for abstraction 226 of hydrogen from the α -position of tetrahydropyran, 227 which yields the radical α -R (cf. Fig. 1), to account 228 for the effects of the cyclic ether group. As α - \dot{R} is the 229 most abundant tetrahydropyranyl isomer, β -scission 230 reactions were updated following theoretical 231 calculations in Rotavera et al. [8]. Given the absence 232 of rate coefficients for tetrahydropyranyl reactions, R 233 + O₂ rate parameters for cyclohexyl + O₂ [23] were 234 adopted because of the similarity in the number of conformers and related axial and equatorial hydrogen atoms. Other reaction classes considered to describe low-temperature combustion are similar to alkanes [24]. To account for the existence of the three R 238 isomers for tetrahydropyran, pre-exponential factors for $\dot{R} + O_2$ were lowered by a factor of ~ 3 for each 241 such that the total rate of \dot{R} + O_2 is similar to Zou et al. [23]. Pre-exponential factors for isomerization reactions of ROO into OOOH were divided by a factor 243 of 2 compared to analogous reactions of cyclohexylperoxy [23]. In addition, elementary 244 reactions of the conjugate alkene isomers were defined in detail following the approach for pentene isomers in NUIGmech1.1 where the most influential reactions were OH-addition to the C=C bond, the 250 Waddington mechanism, hydroxy-alkylperoxy 251 radical reactions, HOO-addition to allylic radicals, and alkenyl-peroxy radical reactions. Polynomial coefficients for thermodynamic properties of species related to tetrahydropyran that are absent in Tran et al. [7] were estimated via group additivity using reaction mechanism generator (RMG) [25, 26]. Mechanism files and a species glossary are in \$4. 257

3. Results

258

259 260

265

270

272

The following sections describe the ignition delay 261 time measurements (Section 3.1) at 10 bar and 20 bar for lean and stoichiometric conditions along with RCM-measured species profiles (Section 3.2). JSR species profiles (Section 3.3) are described at stoichiometric conditions from 500 - 900 K. Modeling predictions for ignition delay times and species profiles are included throughout. Sensitivity 268 analysis at the time of ignition is also included to investigate model discrepancies.

271 Section 3.1 – ignition delay times

Figure 2a compares ignition delay times of tetrahydropyran measured at stoichiometric conditions between 5 bar and 20 bar. The raw, unaveraged data for the ignition delay time measurements are in S1 along with measurements at other conditions that highlight repeatability in the experiments. Starting around 700 K, NTC behavior is observed at both 5 bar and 10 bar noted from the nonlinear trend in the logarithm of ignition delay times with increasing temperature. The model captures trends qualitatively in Fig. 2a, yet shows quantitative discrepancies below 700 K for 5 bar and 10 bar, where total ignition delay times are overpredicted. First stage ignitions are overpredicted at 5 bar, yet are reproduced more accurately at 10 bar. In the same temperature region at 20 bar, however, the model predicts ignition at stoichiometric conditions within experimental uncertainty. The NTC behavior is exaggerated in the experiments at the lower equivalence ratio (Fig. 2b), which coincides with more pronounced discrepancies in the model between 770 K and 900 K. The model predictions of ignition 294 are consistent with the experiments below 730 K at

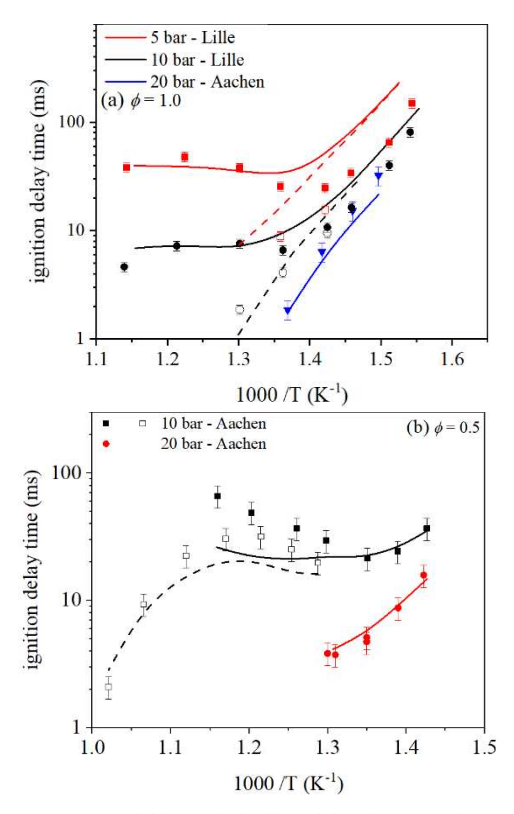


Figure 2. (a) Stoichiometric ignition delay times at 5 bar and 10 bar (Lille), and 20 bar (Aachen); hollow points and experiments denote first-stage ignition. (b) Lean ignition delay times at 10 bar and 20 bar; open symbols and dashed lines denote experiments where Ar is present in the bath gas.

295 lean conditions for 10 bar and 20 bar, yet are shorter 296 in the NTC region; the opposite discrepancy is observed at stoichiometric conditions. Model 298 discrepancies reach a factor of up to ~2.5 near 860 K for lean conditions at 10 bar (Fig. 2b).

301 Section 3.2 –RCM species profiles

Species profiles (\$5) for 14 intermediates were 303 measured in the Lille RCM. The time profile for 304 tetrahydropyran is in Fig. 3. The conjugate alkenes of 305 tetrahydropyran, produced by HOO-elimination from 306 QOOH or by chain-terminating reactions of ROO 307 isomers [8], and propene, which may arise from 308 several pathways, including β -scission reactions of 309 radicals formed via ring-opening, are also in Fig. 3. 310 The model qualitatively reproduces 311 tetrahydropyran profile, yet predicts higher 312 consumption rates after the normalized time of ~ 0.50 . The shape of the time profiles of the alkene 314 intermediates are similar, yet are not well captured by 315 the model, quantitatively. For example, the 316 concentration of 3,4-dihydro-2*H*-pyran decreases at a 317 normalized time of 0.50 in the experiment versus 0.25 318 in the model. The amount of 3,4-dihydro-2*H*-pyran 319 formed at the inflection points are, however,

320 comparable between the experiment and model with

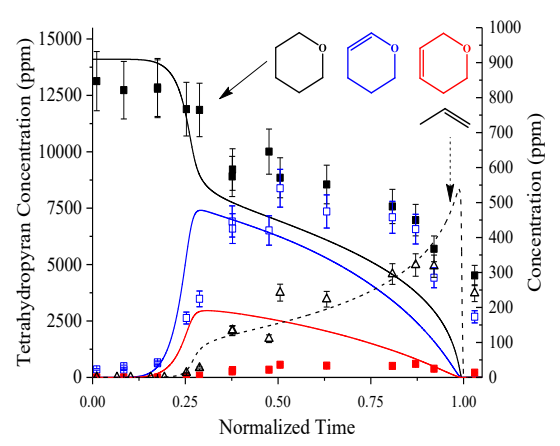


Figure 3: Species time profiles for tetrahydropyran (solid black), 3,4-dihydro-2*H*-pyran (blue), 3,6-dihydro-2*H*-pyran (red), and propene (dashed black and hollow triangles) collected from RCM measurements. Time is normalized to the ignition delay time of 53.4 ms at sampling conditions.

321 concentrations of 540 ppm and 480 ppm respectively. 322 In contrast, 3,6-dihydro-2*H*-pyran concentrations are 323 overestimated up to a factor of 5. The concentration 324 of propene follows a different time profile than the 325 conjugate alkenes of tetrahydropyran and is well-326 captured by the model.

Section 3.3 – JSR Species Profiles

327

328

329

335

Analysis of tetrahydropyran oxidation resulted in the detection of 66 species, 30 of which were 330 quantified and 7 were identified qualitatively (S6). 331 Mass spectra for unidentified intermediates include several which are of parent m/z 98 and m/z 100, and are likely connected to QOOH-mediated pathways (S6). In addition, species were detected in the narrow temperature range of \sim 575 – 625 K, which coincides with ketohydroperoxide formation [10]. From analysis of VUV spectra and mass spectra, 2-methyl-1,3-dioxolane and propyl formate were identified. The 340 formation mechanisms are unclear, vet the 341 temperature profile and molecular structures may from second-O₂-addition reactions 343 decomposition products of ketohydroperoxides (S6). 344 Species profiles for the 30 quantified intermediates are in \$7. The following describes the temperature dependence of intermediates in three sections: tetrahydropyran and conjugate alkene isomers (Section 3.3.1); 1-butyl-derived cyclic ethers (Section 3.3.2); pentanedial and propene (Section 3.3.3).

350 Section 3.3.1 – tetrahydropyran, alkene isomers The temperature dependence of tetrahydropyran 352 and conjugate alkenes products, 3,4-dihydro-2H-353 pyran and 3,6-dihydro-2*H*-pyran, are in **Fig. 4.** Clear 354 NTC behavior is exhibited from 600 - 775 K. The 355 trend is reproduced qualitatively by the model, 356 although not quantitatively due as the predictions 357 show increased consumption and a narrower NTC 358 region, which is predicted to end near 725 K. Both

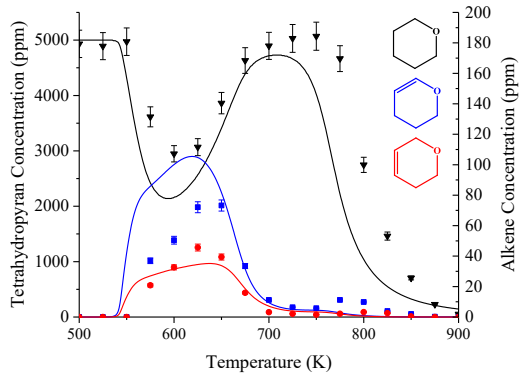


Figure 4: Temperature dependence of tetrahydropyran (black), 3,4-dihydro-2*H*-pyran (blue), and 3,6-dihydro-2*H*pyran (red) at stoichiometric conditions from 500 - 900 K from JSR measurements.

359 3,4-dihydro-2*H*-pyran and 3,6-dihydro-2*H*-pyran 360 reach local maxima in concentration at 625 K and 775 361 K. Steady-state concentrations of 3,4-dihydro-2H-362 pyran are higher than that of 3,6-dihydro-2*H*-pyran, 363 which is consistent with [8]. Prior to the NTC region, 364 the model predicts the magnitude of 3,4-dihydro-2*H*-365 pyran and 3,6-dihydro-2*H*-pyran concentrations 366 within experimental uncertainty (Fig. 4). yet the 367 temperature dependence of the two alkenes is not 368 captured. The model predicts alkene formation at 369 lower temperatures during first-stage ignition and 370 predicts negligible formation in the second stage 371 potentially due to increased rates of tetrahydropyranyl ring-opening reactions.

374 Section 3.3.2 – 1-butyl-derived cyclic ethers

The cyclic ether group in tetrahydropyran enables 376 ring-opening of lpha- $\dot{
m R}$ into pentanal-5-yl 377 (H2C(CH2)3C(=O)H), which undergoes facile 378 isomerization and subsequent decarbonylation to 379 form 1-butyl + CO [10]. No other species that could 380 form from pentanal-5-yl, such as 4-pentenal, were 381 observed. The production of 1-butyl radicals is 382 confirmed by the detection of all three cyclic ethers 383 formed upon reaction with O2: 1,2-epoxybutane, 2-384 methyloxetane, and tetrahydrofuran (Fig. 5).

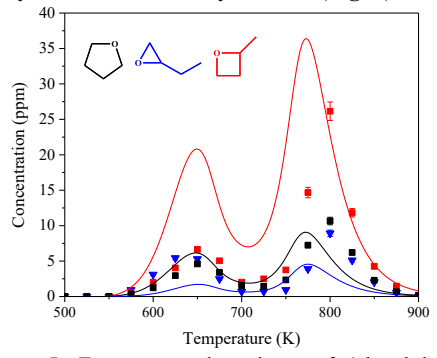


Figure 5: Temperature dependence of 1-butyl-derived cyclic ethers: 1,2-epoxybutane, 2-methyloxetane, and tetrahydrofuran. Modeling results divided by a factor of 10.

385 The reactions in the model describing the formation and consumption of cyclic ethers comes from the base mechanism, NUIGmech1.1. For all cyclic ethers, the model overpredicts the steady-state concentration by an order of magnitude, which may arise from uncertainties in the preceding reaction steps of tetrahydropyran-1-yl leading to 1-butyl.

Section 3.3.3 – pentanedial and propene

393

396

Steady-state concentrations of pentanedial, which forms only from ring-opening of α - α '- $\dot{Q}OOH$ (cf. **Fig.** 394 1) and subsequent loss of OH, reaches local maxima at 650 K and 775 K (Fig. 6). Increased flux towards ring-opening of α - $\dot{\alpha}$ - $\dot{Q}OOH$ coincides with increasing temperature into the NTC region from 600 650 K, which is also observed for the analogous species in tetrahydrofuran oxidation, butanedial [19]. 401 At 700 K, pentanedial concentration reaches a steady-402 state concentration of ~100 ppm, indicating that 403 nearly all of the tetrahydropyran is consumed (cf. Fig. 4) via the chain-propagating pathway. The model incorrectly predicts the temperature dependence of pentanedial, by the 60-K difference in peak concentrations, and quantitatively by a factor of ~ 2.5 . Similar model discrepancies were observed for tetrahydrofuran oxidation for the analogous reaction at nearly the reaction conditions [19].

Figure 6 also shows the temperature dependence 411 412 of propene, which is qualitatively captured by the model. However, quantitative discrepancies up to a factor of 4 exist below 700 K. Propene is formed at temperatures as low as 575 K, where C-C β-scission reaction rates of 1-butyl to form propene are unfavorable compared to reaction with O₂ (vide infra) while a direct pathway from pentanedial exists via successive decarbonylation steps. Additional 420 formation pathways to propene may exist that are not 421 included in the present chemical kinetics mechanism.

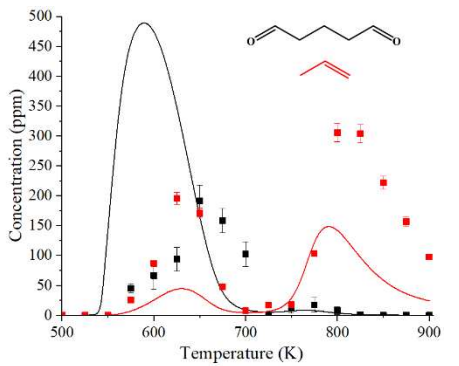


Figure 6: Temperature dependence of pentanedial (black) and propene (red) compared to model predictions (lines).

422 4. Discussion

The first detailed chemical kinetics mechanism to 424 incorporate peroxy-radical reactions was created and 425 compared with ignition delay time and species profile measurements. Ignition delay times of tetrahydropyran are shorter and demonstrate weaker 428 NTC behavior when compared to cyclohexane 429 ignition at similar conditions [27]. The difference in ignition delay indicates increased reactivity caused by 431 the presence of the cyclic ether functional group, 432 which is also observed for tetrahydrofuran, 2-433 methyltetrahydrofuran, and 3-methlytetrahydrofuran 434 when compared to respective alkane analogues [4]. 435 Discrepancies in first-stage ignition predictions of the 436 RCM experiments were observed (Fig. 2) and in the 437 time profiles given the overpredicted consumption of tetrahydropyran near 0.30 on the x-axis in **Fig. 3**. 439 Disagreements between the model and total ignition 440 delay times were most apparent in the NTC region at 441 lean conditions and 10 bar pressure (Fig. 2), although 442 the same region is captured well by the model at 443 stoichiometric conditions. Sensitivity analysis at the 444 time of ignition was conducted on OH concentration 445 at 825 K and 10 bar for stoichiometric, lean, and RCM 446 sampling conditions (S8). The OH concentration was 447 chosen for the sensitivity analysis given the radical directly reflects the predicted reactivity. In all cases, OH shows positive sensitivity to H-abstraction from 450 tetrahydropyran by $\dot{O}H$ and $HO\dot{O}$ to form $\alpha - \dot{R}$, 1-451 butyl formation from ring-opening of α - \dot{R} , and chain-452 branching reactions stemming from 1-butyl + O₂. In 453 contrast, OH sensitivity is negative for H-abstraction 454 by $\dot{O}H$ to form β - \dot{R} , which may undergo ring-opening 455 to form an alkoxy radical via C-O bond-scission 456 along with propagation reactions from 1-butyl to form 457 2-methyloxetane and 1-butene. To model 458 tetrahydropyran oxidation effectively, the sensitivity 459 analysis highlights the necessity of not only capturing 460 the overall rate for $\dot{O}H$ + tetrahydropyran \rightarrow products 461 but also accurately capturing the branching fraction 462 for the distribution of initial radicals, which imposes 463 significant effects on ignition delay time simulations 464 for biofuels when total rate constants are similar. As 465 the H-abstraction reaction rates prescribed in the 466 current mechanism are estimates, an important aspect of model improvement is an accurate set of theoretical calculations.

Given the propensity of α - \dot{R} to undergo ringopening and form pentanal-5-yl, the connection 471 between tetrahydropyran and *n*-butane oxidation 472 becomes clear and shows that fundamental 473 understanding of peroxy-radical reactions in alkanes 474 is also important for modeling cyclic ether combustion. Branching fractions for H-abstraction from linear aldehydes almost exclusively favor the aldehydic carbon site [28]. In the case of pentanal-5-478 yl, favorable intramolecular H-transfer forms pentanal-1-yl, which is then most likely to decompose 480 into 1-butyl + CO via decarbonylation [29]. To the 481 extent that O₂-addition to pentanal-5-yl occurs 482 instead, the same reaction mechanism involving 483 intramolecular H-transfer of the aldehydic H-atom to 484 the peroxy group and subsequent decarbonylation may occur and result in hydroperoxy-but-4-yl, which 486 ties directly to the peroxy-radical reactions explaining 487 the oxidation of 1-butyl. No intermediates that arise 488 exclusively from O₂ + pentanal-5-yl, namely 4-489 pentenal, were observed, which suggests that the

490 primary consumption pathway for pentanal-5-yl leads to the formation of 1-butyl + CO. Flux through the aldehyde-radical pathway allows for the formation of the three cyclic ether intermediates of 1-butyl (cf. Fig. 494 5). The model overpredicts concentrations of the cyclic ethers by nearly an order of magnitude, which 496 from Dewey and Rotavera [30] is attributable in part inadequate description of consumption 497 mechanisms. Uncertainties in the preceding reaction 498 steps leading to 1-butyl likely also contribute to the 499 model discrepancies. Applying the aldehyde-radical pathway to ring-opening of α -tetrahydrofuranyl yields butanal-4-yl and, subsequently, propene + CO [19]. 502 The inclusion of these reactions into the mechanism 504 may reduce the overprediction of tetrahydrofuran concentrations. As the current mechanism is sensitive 506 to chain-branching reactions from 1-butyl oxidation, accurately capturing the profiles for chainpropagating species from 1-butyl is likely crucial to 508 modeling tetrahydropyran. 509

As evident by the relatively high concentration of pentanedial observed in the JSR experiments, ring-512 opening of α - α '- $\dot{Q}OOH$ is yet another pathway that is important to accurately model tetrahydropyran oxidation. The current mechanism prescribes pentanedial consumption to occur exclusively through 516 abstraction of one of the two aldehydic H atoms followed by decarbonylation to form butanal-4-yl. Given the experimental conclusion that the primary pathway for pentanyl-5-yl consumption is 1-butyl formation, a reasonable expectation is that butanal-4-521 yl follows the same pathway to yield 1-propyl + CO. 522 However, the latter reaction is not currently prescribed in the mechanism. Oxidation of 1-propyl 524 overwhelmingly favors the formation of propene [31]. 525 JSR experiments appear to corroborate the presence 526 of 1-propyl as propene is observed even at 575 K where C-C β -scission is unfavorable, which could otherwise account for a portion of propene formation. However, at 575 K, the rate of C–C β -scission of 1propyl is $6.7 \cdot 10^1 \, \text{s}^{-1}$ [32, 33] while the pseudo-firstorder rate of O2 addition, assuming a lower limit of k(T) of 10^{-12} cm³ molecules⁻¹ s⁻¹, is $4.9 \cdot 10^5$ s⁻¹ at stoichiometric conditions and 1 atm.

The time profile of propene is captured well during 535 RCM sampling at 10 bar, indicating that the prescribed mechanism for propene formation is more accurate at higher pressures due to the increase in collision frequency facilitating rates of β -scission reactions. The model currently overpredicts the peak concentration of pentanedial and predicts peak 541 temperature of formation 50-K below the JSR experimental trend. Similar to Dewey and Rotavera 543 for cyclic ethers [30], the addition of an accurate 544 consumption mechanism for butanal-4-yl that includes the pathway to 1-propyl may result in more accurate model predictions at lower pressures for both tetrahydrofuran and pentanedial. Such discrepancies in pentanedial predictions are also observed for 549 butanedial in tetrahydrofuran oxidation [19], at almost 550 the exact same combustion conditions, which may

532

533

Reaction mechanism describing fate of Figure 7: tetrahydropyran-1-yl ring-opening pathways leading via decarbonylation to 1-butyl and 1-propyl radicals. Subsequent reaction of the alkyl radicals with O2 may contribute to chainbranching during tetrahydropyran oxidation.

551 indicate modeling of other biofuels or hydrocarbons 552 might benefit from a similar approach.

Figure 7 summarizes reaction 554 significant to tetrahydropyran combustion, which are 555 elevated in importance due to the favorability of H-556 abstraction at α sites forming \dot{R} and analogous 557 reactions for ROO isomerization to QOOH. The 558 ability for α -radicals to ring-open aids in identifying two deficiencies in the current model, which partially 560 account for the discrepancies in predicted ignition 561 delay times. First, ring-opening of α - \dot{R} creates 562 additional chain-branching pathways from O2-563 addition to QOOH radicals formed from oxidation of 564 1-butyl [34] and 1-propyl [35, 36]. Accurate modeling 565 of the balance of QOOH-mediated pathways remains 566 important, specifically rates for unimolecular 567 pathways, QOOH → products, relative to rates for 568 bimolecular pathways, $\dot{Q}OOH + O_2 \rightarrow products$. For 569 example, an imbalance in the model predictions of 570 concentrations of cyclic ethers that stem from a lack 571 of consumption mechanisms in the model impacts the 572 flux to chain-propagation. For the case where chain-573 propagation rates are artificially lower, increased flux 574 toward chain-branching via 1-butyl-derived or 1-575 propyl-derived QOOH may result. Secondly, the ring-576 opening step of α - α '- $\dot{Q}OOH$ is chain-propagating, yet 577 the most likely consumption mechanism for the stable 578 co-product, pentanedial, is more complex and may lead to chain-branching via second-O2-addition 580 reactions of QOOH derived from 1-propyl [35, 36]. 581 The net effect of the two deficiencies originating from 582 ring-opening is ultimately an increase in the predicted 583 amount of OH and, therefore, increased reactivity 584 (and decreased ignition times).

586 5. Conclusions

Ignition delay times and species profiles were 588 measured in rapid compression machines from 5 bar – 20 bar, spanning several equivalence ratios. Species 590 profiles were also measured in JSR experiments at 1 591 bar and stoichiometric conditions, providing the first 592 set of data on the low-temperature combustion of 593 tetrahydropyran. The measurements were then 594 compared against the first chemical kinetics 595 mechanism for tetrahydropyran developed herein that 596 includes peroxy radical reactions. RCM experiments 597 at lean conditions and 10 bar show the largest 598 difference in predicted reactivity from the first-

generation model. Species profiles and sensitivity analysis indicate that direct calculation of rates for 601 abstraction reactions from tetrahydropyran by both OH and HOO, which are currently estimated from 603 analogy, is required. In addition, rates for competing 604 reactions of tetrahydropyranyl radicals (ring-opening versus O₂-addition) are also required.

Species profiles from the JSR experiments indicate 606 that α - \dot{R} and α - α' - $\dot{Q}OOH$ are major radicals and 607 608 highly susceptible to ring-opening due to the cyclic ether group. Ring-opening reactions lead to aldehyde 610 radical reactions becoming influential, particularly 611 decarbonylation, which connects the combustion of 612 tetrahydropyran to alkyl radicals – because 1-butyl 613 and 1-propyl consumption may contribute to the 614 chain-branching sequence of tetrahydropyran. In multiple 615 aggregate, direct and indirect 616 ketohydroperoxide channels may contribute to chain-617 branching during tetrahydropyran oxidation. Understanding the balance between ring-opening and oxygen addition to both R and QOOH is therefore critical. In addition to prescribing accurate rates for 621 intermediate formation and related thermochemical properties, the addition of detailed consumption 623 mechanisms for the combustion intermediates, such 624 as pentanedial and the conjugate alkene isomers, is 625 also important.

627 Acknowledgements

626

645

647

648

651

655

BR acknowledges support by the National Science 628 629 Foundation (NSF) under Grant No. 2042646 and the 630 Global Research Collaboration program of the 631 University of Georgia Office of Global Engagement. 632 The CaPPA project (Chemical and Physical 633 Properties of the Atmosphere) is funded by the French 634 National Research Agency (ANR) through the PIA 635 (Programme d'Investissement d'Avenir) under 636 contract ANR-11-LABX-0005-01 and by the Regional Council, Hauts-de-France, and the European 638 Funds for Regional Economical Development (FEDER). The work at RWTH Aachen University funded by the Deutsche Forschungsgemeinschaft (DFG, German Research Foundation) 642 under the German Excellence Strategy-Cluster of 643 Excellence 2186, The Fuel Science Center, ID: 644 390919832.

646 Supplementary material

- S1 Mole Fractions and Ignition Delay Times
- S2 Mass and Absorbance Reference Spectra
- 649 S3 – Quantification Methods for JSR Experiments
- S4 Kinetics Model Glossary 650
 - S5 RCM Sampling Species Profiles
- 652 S6 - Extra Information for Observed JSR Products
- 653 S7 – JSR Species Profiles
- S8 Sensitivity Analysis Results 654

656 References

[1] K. Ulonska, A. Voll, W. Marquardt, Screening Pathways 658 for the Production of Next Generation Biofuels, Energy 659 Fuels 30 (2016) 445-456.

- 660 [2] M. J. Climent, A. Corma, S. Iborra, Conversion of 661 biomass platform molecules into fuel additives and liquid 662 hydrocarbon fuels, Green Chem. 16 (2014) 516-547.
- 663 [3] L.-S. Tran, O. Herbinet, H.-H. Carstensen, F. Battin-664 Leclerc, Chemical kinetics of cyclic ethers in combustion,
- 665 Prog. Energy Combust. Sci. 92 (2022) 101019
- 666 [4] B. Rotavera, C. A. Taatjes, Influence of Functional 667 Groups on Low-Temperature Combustion Chemistry of 668 Biofuels, Prog. Energy Combust. Sci. (2021) 100925
- 669 [5] P. Dagaut, M. McGuinness, J. M. Simmie, M. Cathonnet,
- 670 The Ignition and Oxidation of Tetrahydropyran: 671 Experiments and Kinetic Modeling, Combust. Sci. Technol.
- 672 135 (1998) 3-29.
- 673 [6] N. J. Labbe, V. Seshadri, T. Kasper, N. Hansen, P. 674 Oßwald, P. R. Westmoreland, Flame chemistry of 675 tetrahydropyran as a model heteroatomic biofuel, Proc. 676 Combust. Inst. 34 (2013) 259-267.
- 677 [7] L.-S. Tran, R. De Bruycker, H.-H. Carstensen, P.-A. 678 Glaude, F. Monge, M. U. Alzueta, R. C. Martin, F. Battin-679 Leclerc, K. M. Van Geem, G. B. Marin, Pyrolysis and 680 combustion chemistry of tetrahydropyran: Experimental and 681 modeling study, Combust. Flame 162 (2015) 4283-4303.
- 682 [8] B. Rotavera, J. D. Savee, I. O. Antonov, R. L. Caravan, 683 L. Sheps, D. L. Osborn, J. Zádor, C. A. Taatjes, Influence of 684 oxygenation in cyclic hydrocarbons on chain-termination 685 reactions from R + O₂: tetrahydropyran and cyclohexane, 686 Proc. Combust. Inst. 36 (2017) 597-606.
- [9] M.-W. Chen, B. Rotavera, W. Chao, J. Zador, C. A. 688 Taatjes, Direct measurement of OH and HO2 formation in R 689 + O₂ reactions of cyclohexane and tetrahydropyran, *Phys.* 690 Chem. Chem. Phys. 20 (2018) 10815-10825.
- 691 [10] J. C. Davis, A. L. Koritzke, R. L. Caravan, I. O. 692 Antonov, M. G. Christianson, A. C. Doner, D. L. Osborn, L. 693 Sheps, C. A. Taatjes, B. Rotavera, Influence of the Ether 694 Functional Group on Ketohydroperoxide Formation in Cyclic Hydrocarbons: Tetrahydropyran and Cyclohexane, J. 696 Phys. Chem. A 123 (2019) 3634-3646.
- 697 [11] A. Ramalingam, K. Zhang, A. Dhongde, L. Virnich, H. 698 Sankhla, H. Curran, A. Heufer, An RCM experimental and modeling study on CH₄ and CH₄/C₂H₆ oxidation at pressures 700 up to 160 bar, Fuel 206 (2017) 325-333.
- 701 [12] C.-J. Sung, H. J. Curran, Using rapid compression 702 machines for chemical kinetics studies, Prog. Energy 703 Combust. Sci. 44 (2014) 1-18.
- 704 [13] B. W. Weber, C.-J. Sung, M. W. Renfro, On the 705 uncertainty of temperature estimation in a rapid compression 706 machine, Combust. Flame 162 (2015) 2518-2528.
- [14] C. S. Mergulhão, Y. Fenard, G. Kukkadapu, S. W. 708 Wagnon, G. Vanhove, Investigating the kinetic effect of 709 prenol on iso-octane auto-ignition by means of an 710 experimental and modeling study, Fuel 328 (2022) 125225
- 711 [15] N. Bourgeois, S. S. Goldsborough, H. Jeanmart, F.
- 712 Contino, CFD simulations of Rapid Compression Machines 713 using detailed chemistry: Evaluation of the 'crevice
- 714 containment' concept, Combust. Flame 189 (2018) 225-239.
- [16] Y. Fenard, H. Song, H. Minwegen, P. Parab, C. Sampaio
- 716 Mergulhão, G. Vanhove, K.-A. Heufer, 717 Dimethyltetrahydrofuran combustion: Ignition delay times
- 718 at high and low temperatures, speciation measurements and 719 detailed kinetic modeling, Combust. Flame 203 (2019) 341-
- 721 [17] P. Dagaut, M. Cathonnet, J. P. Rouan, R. Foulatier, A. 722 Quilgars, J.-C. Boettner, F. Gaillard, H. James, A Jet-Stirred
- 723 Reactor for Kinetic Studies of Homogeneous Gas-Phase 724 Reactions at Pressures up to Ten Atmospheres (~1 MPa), J.
- 725 Phys. E: Sci. Instrum. 19 (1986) 207-209.

- 726 [18] S. W. Hartness, N. S. Dewey, M. G. Christianson, A. L.
- 727 Koritzke, A. C. Doner, A. R. Webb, B. Rotavera, Probing O2
- 728 dependence of hydroperoxy-butyl reactions via isomer-
- 729 resolved speciation, Proc. Combust. Inst. 39 (2023) 405-414.
- 730 [19] A. L. Koritzke, N. S. Dewey, M. G. Christianson, S.
- 731 Hartness, A. C. Doner, A. R. Webb, B. Rotavera, Probing
- 732 O2-dependence of tetrahydrofuranyl reactions via isomer-
- 733 resolved speciation, Combust. Flame 257 (2023)
- 734 [20] A. Ramalingam, S. Panigrahy, Y. Fenard, H. Curran, K. 735 A. Heufer, A chemical kinetic perspective on the low-
- 736 temperature oxidation of propane/propene mixtures through
- 737 experiments and kinetic analyses, *Combust. Flame* 223
- 738 (2021) 361-375.
- 739 [21] A. M. Dean, J. W. Bozzelli, in: Gas-Phase Combustion
- 740 Chemistry, W. C. Gardiner, (Ed.) Springer New York: New
- 741 York, NY, 2000; pp 125-341.
- 742 [22] S. M. Handford-Styring, R. W. Walker, Arrhenius
- 743 parameters for the reaction HO₂+cyclohexane between 673
- 744 and 773 K, and for H atom transfer in cyclohexylperoxy 745 radicals, *Phys. Chem. Chem. Phys.* 3 (2001) 2043-2052.
- 746 [23] J. Zou, Y. Li, L. Ye, H. Jin, A comprehensive study on
- 747 low-temperature oxidation chemistry of cyclohexane. I.
- 748 Conformational analysis and theoretical study of first and
- 749 second oxygen addition, Combust. Flame 235 (2022)
- 750 111550
- 751 [24] H. J. Curran, P. Gaffuri, W. J. Pitz, C. K. Westbrook, A
- 752 comprehensive modeling study of n-heptane oxidation,
- 753 Combust. Flame 114 (1998) 149-177.
- 754 [25] M. S. Johnson, X. Dong, A. Grinberg Dana, Y. Chung,
- 755 D. Farina, Jr., R. J. Gillis, M. Liu, N. W. Yee, K. Blondal, E.
- 756 Mazeau, C. A. Grambow, A. M. Payne, K. A. Spiekermann,
- 757 H. W. Pang, C. F. Goldsmith, R. H. West, W. H. Green,
- 758 RMG Database for Chemical Property Prediction, *J Chem* 759 *Inf Model* 62 (2022) 4906-4915.
- 760 [26] M. Liu, A. Grinberg Dana, M. S. Johnson, M. J.
- 761 Goldman, A. Jocher, A. M. Payne, C. A. Grambow, K. Han,
- 762 N. W. Yee, E. J. Mazeau, K. Blondal, R. H. West, C. F.
- 763 Goldsmith, W. H. Green, Reaction Mechanism Generator
- 764 v3.0: Advances in Automatic Mechanism Generation, J
- 765 Chem Inf Model 61 (2021) 2686-2696.
- 766 [27] S. Vranckx, C. Lee, H. K. Chakravarty, R. X.
- 767 Fernandes, A rapid compression machine study of the low
- 768 temperature combustion of cyclohexane at elevated
- 769 pressures, Proc. Combust. Inst. 34 (2013) 377-384.
- 770 [28] M. Pelucchi, S. Namysl, E. Ranzi, A. Frassoldati, O. 771 Herbinet, F. Battin-Leclerc, T. Faravelli, *Proc. Comb. Inst.*
- 771 Heromet, F. Battin-Lecterc, T. Faraveill, *Froc. Comb. Inst*
- 772 37 (2019) 389-397.
- 773 [29] M. Pelucchi, E. Ranzi, A. Frassoldati, T. Faravelli,
- 774 Alkyl radicals rule the low temperature oxidation of long
- 775 chain aldehydes, *Proc. Combust. Inst.* 36 (2017) 393-401.
- 776 [30] N. S. Dewey, B. Rotavera, Reaction mechanisms of
- 777 alkyloxiranes for combustion modeling, *Combust. Flame* 778 252 (2023)
- 779 [31] O. Welz, M. P. Burke, I. O. Antonov, C. F. Goldsmith,
- 780 J. D. Savee, D. L. Osborn, C. A. Taatjes, S. J. Klippenstein,
- 781 L. Sheps, New Insights into Low-Temperature Oxidation of
- 782 Propane from Synchrotron Photoionization Mass
- 783 Spectrometry and Multiscale Informatics Modeling, *The* 784 *Journal of Physical Chemistry A* 119 (2015) 7116-7129.
- 785 [32] J. A. Kerr, A. F. Trotman-Dickenson, The reactions of
- 786 alkyl radicals. Part III. n-Butyl radicals from the photolysis
- 787 of n-valeraldehyde, Journal of the Chemical Society
- 788 (Resumed) (1960) 1602-1608.
- 789 [33] H. J. Curran, Rate constant estimation for C1 to C4 alkyl
- 790 and alkoxyl radical decomposition, Int. J. Chem. Kinet. 38
- 791 (2006) 250-275.

- 792 [34] A. J. Eskola, O. Welz, J. Zádor, I. O. Antonov, L. Sheps,
- 793 J. D. Savee, D. L. Osborn, C. A. Taatjes, Probing the low-
- 794 temperature chain-branching mechanism of n-butane 795 autoignition chemistry via time-resolved measurements of
- 796 ketohydroperoxide formation in photolytically initiated n-
- 797 C₄H₁₀ oxidation, *Proc. Combust. Inst.* 35 (2015) 291-298.
- 798 [35] C. F. Goldsmith, W. H. Green, S. J. Klippenstein, Role
- 799 of O2 + QOOH in Low-Temperature Ignition of Propane. 1. 800 Temperature and Pressure Dependent Rate Coefficients, J.
- 801 of Phys. Chem. A 116 (2012) 3325-3346.
- 802 [36] S. S. Merchant, C. F. Goldsmith, A. G. Vandeputte, M.
- 803 P. Burke, S. J. Klippenstein, W. H. Green, Understanding
- 804 low-temperature first-stage ignition delay: Propane,
- 805 Combust. Flame 162 (2015) 3658-3673.